Physics of Fluids

Oscillating grid turbulence in shear-thinning polymer solutions

Cite as: Phys. Fluids **31**, 083102 (2019); https://doi.org/10.1063/1.5113551
Submitted: 05 June 2019 . Accepted: 18 July 2019 . Published Online: 12 August 2019

T. Lacassagne, S. Simoëns, M. EL Hajem, A. Lyon, and J.-Y. Champagne

COLLECTIONS

This paper was selected as an Editor's Pick

View Online Export Citation CrossMark

ARTICLES YOU MAY BE INTERESTED IN

Large-eddy simulation of turbulent natural-bed flow
Physics of Fluids **31**, 085105 (2019); https://doi.org/10.1063/1.5116522

Analytical solutions of incompressible laminar channel and pipe flows driven by in-plane wall oscillations
Physics of Fluids **31**, 083605 (2019); https://doi.org/10.1063/1.5104356

Interaction of cylindrical converging shocks with an equilateral triangular SF_6 cylinder
Physics of Fluids **31**, 086104 (2019); https://doi.org/10.1063/1.5094671

AIP Author Services
English Language Editing

AIP Publishing

© 2019 Author(s).

Physics of Fluids ARTICLE scitation.org/journal/phf

Oscillating grid turbulence in shear-thinning polymer solutions

Cite as: Phys. Fluids 31, 083102 (2019); doi: 10.1063/1.5113551
Submitted: 5 June 2019 • Accepted: 18 July 2019 •
Published Online: 12 August 2019

View Online Export Citation CrossMark

T. Lacassagne,[a] S. Simoëns,[b] M. EL Hajem, A. Lyon, and J.-Y. Champagne

AFFILIATIONS

Univ Lyon, INSA Lyon, Ecole Centrale de Lyon, Université Claude Bernard Lyon I, CNRS, LMFA, UMR 5509, 20 avenue Albert Einstein, F-69621, Villeurbanne, France

[a]Electronic mail: tom.lacassagne@gmail.com
[b]Electronic mail: serge.simoens@ec-lyon.fr

ABSTRACT

Oscillating grid apparatuses are well known and convenient tools for the fundamental study of turbulence and its interaction with other phenomena since they allow to generate turbulence supposedly homogeneous, isotropic, and free of mean shear. They could, in particular, be used to study turbulence and mass transfer near the interface between non-Newtonian liquids and a gas, as already done in air-water situations. Although frequently used in water and Newtonian fluids, oscillating grid turbulence (OGT) generation has yet been rarely applied and never characterized in non-Newtonian media. The present work consists of a first experimental characterization of the flow properties of shear-thinning polymer (Xanthan Gum, XG) solutions stirred by an oscillating grid. Various polymer concentrations are tested for a single grid stirring condition. The dilute and semidilute entanglement concentration regimes are considered. Liquid phase velocities are measured by Particle Image Velocimetry. The existing mean flow established in the tank is described and characterized, as well as turbulence properties (intensity, decay rate, length scales, isotropy, etc.). OGT in dilute polymer solutions induces an enhanced mean flow compared to water, a similar decay behavior with yet different decay rates, and enhanced turbulence large scales and anisotropy. In the semidilute regime of XG, turbulence and mean flows are essentially damped by viscosity. The evolution of mean flow and turbulence indicators leads to the definition of several polymer concentration subregimes, within the dilute one. Critical concentrations around 20 ppm and 50 ppm are found, comparable to drag reduction characteristic concentrations.

Published under license by AIP Publishing. https://doi.org/10.1063/1.5113551

I. INTRODUCTION

Oscillating grid stirred tanks have been used for many purposes in research on turbulence, for example, the study of interactions between turbulence and solid impermeable boundaries,[1,2] in stratified media,[3–6] or to study the behavior of bubbles, cells, fibers, and aggregates suspended in a turbulent liquid phase.[7–10]

Such devices are said to generate quasihomogeneous and isotropic turbulence in horizontal planes (parallel to the grid) and to yield theoretically no mean flow, which is their major advantage compared to fixed grid setups. The absence of a strong mean shear avoids the destruction of complex fluids' components (fibers, polymer chains, and cells) that is sometimes observed in fixed grid turbulence.[11] The fact that turbulent structures are theoretically not advected by any mean flow makes them more easily observable by advanced optical techniques such as PIV and PLIF (Planar Laser Induced Fluorescence). It will yet be shown hereinafter that the validity of this no-mean flow assumption is limited without any reduction of turbulent properties. Note that when a mean flow does exist in oscillating grid systems, it takes the shape of a set of stationary recirculation patterns, as will be extensively discussed in this work. The term "mean flow" will hereinafter refer to this recirculation, which can sometimes be called "secondary recirculation" in the literature.

For the previous reasons, this type of device has been extensively used for the study of turbulence and gas-liquid mass transfer at free surfaces.[12–15] The combination of numerical simulations[16–18] and experiments[19–23] has allowed to describe the behavior of turbulence close to a flat air-water interface and the influence of this near surface turbulence on the fundamental and local mechanisms of gas dissolution into the liquid phase. Yet, these mechanisms are known to be modified when considering gas dissolution into a

Published under license by AIP Publishing

non-Newtonian or surfactant-laden liquid phase. The influence of surface contamination by surface active agents has already been the subject of numerical simulations[24,25] and experimental works,[13] but the effect of bulk fluid rheological properties remains to be understood. This phenomenon is of great interest since it is frequently encountered in the chemical, pharmaceutical, and process industries.[26–28] In this context, experiments of non-Newtonian turbulence's interactions with flat free interfaces are still needed. The convenience of oscillating grid setups, often used in air-water situations, makes them interesting candidates for such experiments.

Only a few studies of oscillating grid turbulence (OGT) with non-Newtonian liquids can be found in the literature,[29–31] and none of them seems to tackle the effects of variable viscosity on the possible mean flow and turbulence properties mapping in the whole tank. Moreover, these studies focus on turbulence below the grid, between the sweep region and the bottom of the tank, for which the boundary condition and thus mean flows are inherently different from the application considered here. The aim of this paper is to study the influence of a shear thinning behavior on the hydrodynamics above the grid and below a free surface in an oscillating grid stirred tank, as a first necessary step for a further investigation of near surface turbulence and mass transfer in similar fluids. Such properties are given to an initially Newtonian fluid, water, by addition of a minute amount of polymer (Xanthan Gum, XG). Fluid velocity measurements are achieved using Particle Image Velocimetry (PIV) in a region of the tank located between the upper position of the grid and the free surface.

The objective is to describe OGT precisely in shear thinning polymer solutions and see if its velocity field statistical properties can be compared to OGT in water. In other words, can this device be used to generate controlled turbulence in such fluids, and does the hypothesis of a negligible mean flow remain valid? An underlying question is: can an oscillating grid apparatus be used to study turbulence near a free surface in shear thinning polymer solutions? To do so, indicators of turbulence and mean flow topology are extracted. The effects of polymer concentration on the existing mean flow topology are first studied. The evolution of turbulence properties with the distance from the grid and polymer concentration is then addressed. Finally, possible causes for the apparent mean flow enhancement are discussed, and the different concentration regimes evidenced are compared to drag reduction characteristics of XG.

II. BACKGROUND

A. Oscillating grid turbulence in Newtonian liquids

The principle of an oscillating grid apparatus is to produce turbulence by making a grid oscillate at a frequency f and with an amplitude or stroke S. It is commonly said that the jets and wakes behind the grid's holes and bars interact to generate turbulence,[3,4,14,32] which then diffuses away from the grid. Turbulence can be studied either above[4] or below the grid,[6] the bottom boundary condition being a rigid wall and the top boundary condition being either a rigid wall[3] or a free surface.[20] The first oscillating grid apparatus were designed by Rouse and Dodu[33] and Bouvard and Dumas,[34] but full characterization of OGT in prismatic tanks only came with the pioneer works of Thompson and Turner[3] and Hopfinger and Toly[4] (that are referred to as TT and HT, respectively, later in the manuscript).

1. Turbulence properties

When fulfilling a set of conditions on the grid shape, solidity, and distance from the bottom of the tank defined by the previous authors, OGT is supposed to yield a quasihomogeneous and isotropic turbulence with negligible mean flow. Homogeneity and isotropy are achieved in horizontal planes, far enough from the walls and from the grid's extreme positions (2 or 3 times the mesh size M defined below, depending on the study).

Expressions for the root mean square (rms) of horizontal and vertical velocity fluctuations, denoted u'_x and u'_z, respectively, as a function of the distance from the grid z have been derived by Hopfinger and Toly, respectively, [4] as

$$\begin{aligned} u'_x &= C_{1_{HT}} \cdot f \cdot S^{1.5} \cdot M^{0.5} \cdot z^n, \\ u'_z &= C_{2_{HT}} \cdot u'_x, \end{aligned} \tag{1}$$

where f is the grid frequency, S the amplitude of oscillations (or Stroke), and M the mesh size. An expression for the evolution of the horizontal integral length scale of turbulence L with z comes from the work of Thompson and Turner[3]

$$L = C_{TT} \cdot z, \tag{2}$$

where, $C_{TT} \simeq 0.1, C_{1_{HT}} \simeq 0.25$, $C_{2_{HT}} \simeq 1.2$, and $n = -1$ in the original works. These relationships have been verified by a number of studies.[5,6,12,14,35–39] The values of the different constants vary among the works in the following ranges: $C_{TT} \in [0.1 \ldots 0.4]$, $C_{1_{HT}} \in [0.2 \ldots 0.3]$, $C_{2_{HT}} \in [1.1 \ldots 1.4]$. The proportionality coefficient between the integral length scale and the distance to the grid C_{TT} was also found to depend on the S/M ratio.[4,40]

It should also be noted that the previous laws are valid for turbulence both above and below the grid,[4,6] regardless of the boundary condition, except at the vicinity of either the liquid/solid or liquid/gas interface where turbulence is affected by boundary layer interactions.[1,2,12,23] However, mean flow patterns that develop in the tank should depend on boundary conditions. In this work, we will more specifically focus on the case of the flow above the grid and below a free surface.

2. Mean flow

At first, the concept of OGT generating no mean flow, but only isotropic and homogeneous turbulence, was rather well believed. With the development of PIV techniques allowing further spatial investigations of the flow inside OGT tanks, it became clear that a mean flow is always established, even while matching the previous requirements. McKenna and McGillis[41] showed the existence of persistent mean flow structures, with a relative high kinetic energy level as compared to the turbulent kinetic energy. Moreover, this mean flow seems to be poorly repeatable and strongly dependent on initial conditions.[14] It is therefore really hard to predict the mean flow that could occur in the oscillating tank during a specific measurement, and this is one of the main limitations of OGT systems. Oscillating grid apparatus should thus be seen as ways of generating controlled turbulence with low mean flow rather than as a tool to produce completely mean shear free, homogeneous, and isotropic turbulence. McCorquodale and Munro[42] recently suggested a method for reducing mean flows in OGT using an inner box placed inside the stirred

Published under license by AIP Publishing

tank to separate the wall-induced vortices from the rest of the flow. This will be discussed in Sec. V B.

Nevertheless, it is important to point out that all the previous conclusions are yet only valid and established when considering OGT in water (or other Newtonian fluids). Characterization of turbulence velocity fluctuations and integral length scales and evidence of mean flows associated with OGT in shear thinning polymer solutions are yet to be performed. This is the scope of this study. In order to understand the changes that may arise upon polymer addition, the following paragraphs briefly summarize the literature of turbulence in polymer solutions. Studies involving grid turbulence in polymer solutions are detailed in Sec. II C.

B. Drag reduction and turbulence in polymer solutions

It has been known since the late 1940's[43] that a very small concentration of polymer diluted in a solvent could drastically reduce drag. This phenomenon is called drag reduction since it may decrease the pressure drop in a pipe by up to 80%.[44] As it is of paramount interest in many applications such as hydraulics systems or oil and gas industry, a huge number of studies have already addressed this topic.[45]

Since OGT is driven both by large scale motion of the grid and by boundary layer interactions at the grid's bar level, drag reduction should be one of the mechanisms at the origin of the modification of flow properties by the polymer. The basic principle is that the polymer molecules introduced in the solvent act as molecular springs, undergoing coil-stretch transition thus storing part of the kinetic energy of the flow.[46,47] This is especially efficient in high shear regions close to the walls and leads to an apparent increase in the buffer layer thickness of the boundary layer and a drastic reduction of the friction. For a given concentration of polymer, the friction coefficient variations as a function of the Reynolds number departs from the classical Prandtl-Karman law when reaching an onset Reynolds number. This is called the onset of drag reduction.[47] The higher the polymer concentration, the lower the Reynolds number at the onset. When further increasing Re after the onset, the friction factor decreases extremely rapidly until it reaches an asymptotic trend. Depending on the nature of the polymer, two types of drag reduction leading to two asymptotic slopes are possible. In type A drag reduction, the friction coefficient tends to what is called the maximum drag reduction asymptote empirically determined by Virk[48] (see Ref. 47, Fig. 1). In type B drag reduction, it ultimately follows a Prandtl-Karman slope shifted toward lower friction coefficients.[49] The drag reduction level of this last curve is fixed by the polymer concentration. Type A is characteristic of flexible random coiled and highly deformable polymer chains (e.g., PolyEthylene Oxide, PEO) and type B of relatively rigid, elongated, and undeformable molecules. XG studied here is of this second type.[50] This last observation stresses the importance of polymer conformation and rigidity in its interactions with the flow.

The physical mechanisms of drag reduction rely on the interactions between polymer chains and the flow, and the scales at which polymers can take or give energy to the fluid. Polymer chains' structures give them the ability to deform elastically and store energy at small scales,[46] which tends to truncate or modify the flow energy cascade before reaching the Kolmogorov scale.[51–55] Such interactions should also impact turbulence in the homogeneous isotropic case, without high shear and boundary layers effects. It has been shown from direct numerical simulations[56,57] and experiments[53,58–60] that the Eulerian quantities of the bulk turbulence (strain, enstrophy, Reynolds stress, and velocity gradients fields) are strongly reduced at small scales in viscoelastic solutions. The same conclusions can also be drawn using an experimental Lagrangian approach. Crawford *et al.*,[61] for example, performed time resolved measurement of Lagrangian acceleration of tracer particles in a *washing-machine* turbulence and found that the rms and isotropy of particle accelerations were substantially decreased in dilute polymer solutions as compared to water. Viscous dissipation is reduced as the dissipation by the polymer chain increases: polymer chains store energy at small scales and so the small scales of turbulence are damped. But the effect of polymer also propagates to larger scales. This can translate, for example, into an increase of integral length scales and of large scale fluctuations of velocity.[56,59,60] This is also the case in inelastic shear-thinning solutions.[62] Nguyen *et al.*[55] recently studied the flow-polymer interactions in the dissipative range and showed that the polymer pumps energy at a small scale when it is deformed by flow structures and can give back a part of this energy to the flow when relaxing, thus explaining the up-scale propagation observed experimentally. As for OGT, we should thus expect an influence of the polymer on the large scale flow patterns. This is indeed described in Sec. IV A.

In channels or pipes, most of the strain field to be reduced can be found near the walls, and the forcing is done at small scales

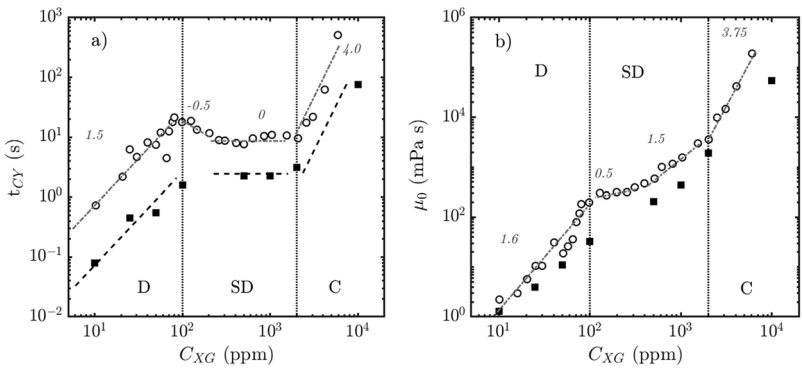

FIG. 1. Evolution of characteristic time scale t_{CY} (a) and zero shear rate viscosity μ_0 (b) with polymer concentration C_{XG}. Data and trends for the present study (respectively, full squares and dashed lines) are compared to the work of Wyatt and Liberatore[76] (empty circles and dashed-dotted lines, for which the slopes are indicated by italic numbers). Dilute (D), semidilute (SD), and concentrated (C) concentration regimes are separated by dotted lines at C_{XG} = 100 ppm and C_{XG} = 2000 ppm on both subfigures.

Published under license by AIP Publishing

(roughness of the wall); hence, the polymer effects are felt at low concentrations, typical of drag reduction. For example, Cai *et al.*[63] observed that viscoelasticity strongly decreased both the frequency and the intensity of burst events generated at the bottom of a channel flow by inhibiting the small scale coherent structures in the sheared sublayer. However, when forcing turbulence by energy injection at scales larger than the cutoff scale, polymers do not play a role at the turbulence production step, and non-Newtonian effects are found to appear for concentrations larger than typical drag reduction concentrations.[59] Finally, an interesting feature observed in flows with strong mean shears such as channel flows[63,64] is an increase of turbulence anisotropy. It comes from the tendency of polymer chains to align with the main shear direction, leading to an increase in tangential velocity fluctuations and a decrease in the normal ones. This effect was lately observed to happen during the propagation of a turbulent/nonturbulent interface as well, where polymer chains tend to align with the turbulent front.[57] Apart from elasticity, shear-thinning induced by the presence of polymer chains is also known to affect many features of flows, turbulent or not, from large to small scales, as described recently in several works.[62,65,66]

C. Grid turbulence in polymer solution

The influence of non-Newtonian behavior on grid turbulence has been mainly studied for fixed grid configuration.[44,67–71] It was found that grid turbulence for such fluids was much more anisotropic, as expected from flows with a preferential shear direction, but also that it decayed more slowly. Recently, Vonlanthen and Monkewitz[11] used PIV measurements to look at turbulent spectra and scales in grid turbulence of dilute polymer solutions and evidence high Reynolds number viscoelastic turbulence. In their experiments, they found that both the shape of the energy spectrum and the elastic ("Lumley") scale evolved with time, which they explained by the destruction of polymer chains by the strong shears in the vicinity of the grid. This shows one of the limits of fixed grid devices for the study of turbulence in polymer solutions: reaching high levels of turbulence requires high flow rates which may cause important degradation of the polymer throughout the measurements. One may thus prefer using OGT rather than fixed grid.

Citing Vonlanthen and Monkewitz,[11] "*The difference between the effect of polymers on turbulence without and with mean shear is that in the former case, the polymers can only provoke additional local energy dissipation, while in the latter case, they can in addition modify the mean shear and with it long-range energy exchange by instabilities.*" The non-Newtonian properties of the fluid are in such a way supposed to affect the OGT turbulence decay law since they act on local turbulence dissipation. The previous sentence also implies that the secondary flows inside the grid stirred tank are very likely to be different in dilute polymer solution than for the Newtonian case.

The first study of OGT in viscoelastic dilute polymer solutions (PEO) was made by Liberzon *et al.*,[29] who observed the velocity propagation of the boundary between turbulent and nonturbulent regions in the tank, at the first instants after the onset of the grid's oscillations. They found that the turbulent/nonturbulent interface moved globally faster in the dilute polymer solution than in water. However, the characteristics of turbulence and mean flow in a steady state are not mentioned, and the author later admitted that results could have been contaminated by the presence of mean shear at the walls of the tank (i.e., by the unexpected mean flow).[57]

Wang *et al.*,[30,31] later used a two oscillating grid device to study the viscoelastic effects of surfactants and dilute polymer on coherent structures. They confirmed that the addition of polymer tends to decrease the small scale effects of turbulence and that this decrease cannot only be attributed to the overall viscosity increase since it is not associated with a decrease of the turbulent kinetic energy. The non-Newtonian property of the flow seemed to strongly modify the spectrum of turbulent structures at large wave numbers. They also found that the turbulent small scale suppression effect arose only when reaching a critical polymer concentration (unfortunately not quantified), which may not be the same in OGT than in channel flows or fixed grid experiments, and seems to be higher than the critical concentration for drag reduction effects.

To our best knowledge, no existing study mentions the possible mean flow that could have developed in grid stirred tanks, and even less its probable polymer concentration dependency. Moreover, the previous studies focused on the case of a viscoelastic polymer solution, while the fluid studied here is shear thinning and inelastic. The evolution of stationary turbulence properties with the distance from the grid, such as turbulent kinetic energy and velocity fluctuations rms, also remain unknown in single oscillating grid systems with dilute polymer solutions (e.g., can profiles analog to HT's law 1 be exhibited?). The aim of this work is thus to characterize both these turbulence properties and the mean flow that possibly establishes in the tank.

III. MATERIALS AND METHODS

A. Polymer solutions

Shear-thinning properties are conferred to the liquid by addition of Xanthan Gum (XG), into distilled water. Here, XG produced by Kelco under the commercial name Keltrol CG-T is used. Its average molar mass is $M_w = 3.4 \times 10^6$ g mol^{-1} and its polydispersity equal to 1.12.[72] XG is chosen for its high resistance to strong shear and extreme temperature and pH conditions.[73] Such features are useful when using it nearby a rigid oscillating grid (which can locally crate high shears), and for future studies of scalar transfer at gas-liquid interfaces.[74] The rheological properties of such solutions have been measured using a MCR 302 Anton Paar Rheometer. Their shear thinning behavior is modeled by a Carreau-Yasuda (CY) equation

$$\frac{\mu - \mu_\infty}{\mu_0 - \mu_\infty} = \left(1 + (t_{CY}\dot{\gamma})^a\right)^{\frac{p-1}{a}}, \tag{3}$$

where the zero shear rate and infinite shear rate Newtonian viscosities (respectively μ_0 and μ_∞), characteristic time scale t_{CY}, and exponents a and p depend on the polymer concentration C_{XG}. The power law decay exponent of viscosity with the increasing shear rate is (p – 1). a is a parameter for the transition between power law and Newtonian behaviors. Their values are reported in Table I for C_{XG} variations over 3 decades.

Published under license by AIP Publishing

TABLE I. Carreau-Yasuda fitting parameters for the shear thinning behavior of XG solutions at various concentrations.

C_{XG} (ppm)	μ_0 (mPa)	μ_∞ (mPa)	t_{CY} (s)	a	p
10	1.30×10^0	0.99	0.08	2.00	0.60
25	3.97×10^0	0.95	0.45	2.00	0.57
50	1.09×10^1	1.09	0.55	2.00	0.50
100	3.28×10^1	1.05	1.60	2.00	0.50
500	2.03×10^2	1.05	2.23	1.27	0.45
1 000	4.43×10^3	1.13	2.23	0.93	0.38
2 000	1.94×10^3	2.73	3.15	0.72	0.25
10 000	5.50×10^4	3.73	75.44	2.00	0.28

By plotting the evolution of the characteristic time scale with polymer concentration (Fig. 1), one can clearly evidence the three main entanglement concentration domains for XG in aqueous salt-free solutions defined by Cuvelier and Launay[75] and Wyatt and Liberatore.[76]

- The dilute regime (D) in which the interaction between isolated polymer chains and the flow are dominant and interactions of polymer chains between each other are negligible.
- The semidilute (SD) regime, in which the electrostatic and mechanical interactions between molecule becomes significant
- The concentrated (C) regime, for which chain entanglement is the dominant mechanism of the liquid phase rheology.

The transition concentration between the three regimes are identical to the ones observed by Wyatt and Liberatore,[76] and so are the zero shear rate viscosity magnitudes. Time scales measured for the present study are typically one order of magnitude lower. This is explainable by the fact that the properties of XG are very sensitive to the molar mass M_w of the polymer, which depends itself on production and dissolution conditions.[73] Moreover, in order to avoid the formation of disordered chains during dissolution, and ensure the reproducibility of measurements, special care has to be taken in the process of dissolving XG. Only distilled water is used without adding any salt, and moderate stirring and heating conditions are applied as specified by Garcia-Ochoa *et al.*[73] In this rheological characterization, the uncertainty on C_{XG} is of the order of 1%. The procedure used for the fabrication of XG solutions for PIV experiments yields uncertainty up to 10% on C_{XG} (see Ref. 74, Appendix A). The associated horizontal error bars are not shown on following figures in the interest of clarity, but this uncertainty has to be kept in mind, especially when discussing critical polymer concentrations in Sec. V A. In this work, the concentration range between 0 and 500 ppm is explored. The focus is made on the dilute regime. The onset of the semidilute regime is also considered, but no measurement is performed in the inner semidilute regime evidenced by Wyatt and Liberatore[76] between 100 ppm and 200 ppm [see Fig. 1(a)], slope equal to −0.5.

B. Oscillating grid setup

Turbulence is generated in a transparent tank of a 277 mm by 277 mm inner cross section. The fluid height is set at H_f = 450 mm and the distance between the surface and the average grid position is 250 mm. The vertical axis, oriented upwards, is noted z, and x and y are the axis defined by the grid bars. The origin of the reference frame is placed at the grid average position (z = 0) at the crossing between the two central bars. In this study, only polymer concentration is varied and all oscillations parameters are kept constant. The grid has square section bars of width equal to 7 mm, and the mesh parameter (distance between two grid bars) is M = 35 mm. This yields a solidity of 0.36, below the maximum value of 0.4 recommended by Thompson and Turner.[3] The frequency is fixed at f = 1 Hz and the stroke at S = 45 mm. It allows us to define a grid-based Reynolds number using the definition of Janzen *et al.*,[20] using the zero shear rate viscosity

$$Re_g = \frac{\rho f S^2}{\mu_0}. \tag{4}$$

TABLE II. Evolution of several properties (De, n, $C_{2_{HT}}$) and indicators ($\overline{\Omega}$, H) with polymer concentration. H is the average of H_z^x over z.

C_{XG} (ppm)	Re_g	De	$\overline{\Omega}$ (1/s)	−n (* or −n′)	$C_{2_{HT}}$	H
0	2.03×10^3	0	2.57	1.0 ± 0.3	1.1 ± 0.4	0.10 ± 0.03
10	1.56×10^3	0.08	2.01	0.7 ± 0.1	1.2 ± 0.1	0.08 ± 0.02
18	7.43×10^2	0.28	2.69	0.72 ± 0.08	1.1 ± 0.2	0.08 ± 0.02
25	5.10×10^2	0.45	2.42	0.89 ± 0.06	1.3 ± 0.1	0.10 ± 0.03
35	3.00×10^2	0.49	3.20	0.88 ± 0.09	1.2 ± 0.1	0.08 ± 0.02
50	1.85×10^2	0.55	3.10	0.9 ± 0.2	1.6 ± 0.3	0.11 ± 0.02
75	9.26×10^1	1.06	4.70	1.1 ± 0.2	1.5 ± 0.3	0.13 ± 0.01
100	6.18×10^1	1.60	5.02	1.2 ± 0.2	1.4 ± 0.3	0.11 ± 0.03
150	3.74×10^1	1.60	5.37	1.5 ± 0.2	1.6 ± 0.4	0.13 ± 0.03
250*	2.10×10^1	1.60	2.31	2.1 ± 0.2	3 ± 1	0.14 ± 0.04
500*	9.97×10^0	1.60	1.30	2.2 ± 0.5	3 ± 1	0.10 ± 0.06

Published under license by AIP Publishing

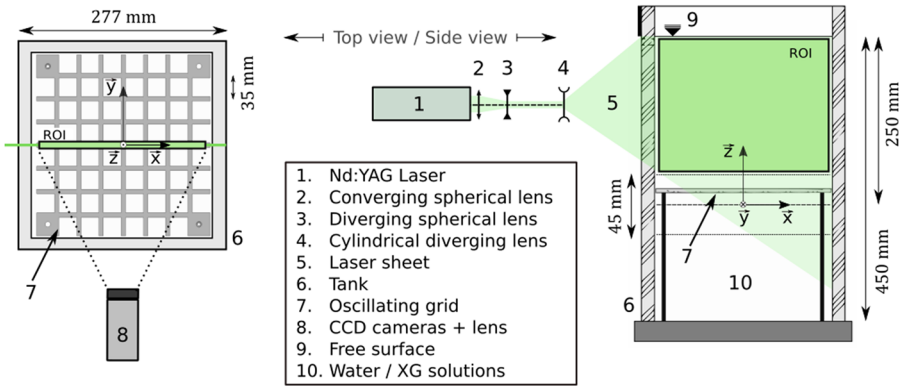

FIG. 2. Sketch of the oscillating grid and PIV setup.

The density ρ of the fluid is assumed equal to that of water because of the very small mass of polymer added. For this range of grid Reynolds number, it has been checked that polymer chains are indeed not destroyed during the experiments (maximum 2 h of duration) by comparing viscosity curves of the solution before and after the experiment. Finally, in order to quantify the ratio between the polymer relaxation time scale and the grid forcing time scale, the grid based Deborah number De is defined as

$$De = \frac{t_{CY}}{T} = t_{CY} f \tag{5}$$

with T the period of oscillations. Values of Re_g and De are reported in Table II for each concentration studied.

C. PIV measurements

Liquid phase velocity measurements in the tank are achieved by Particle Image Velocimetry (PIV). The experimental setup is sketched in Fig. 2. The region of interest (ROI) is a vertical rectangle, in plane $(\vec{x}, \vec{z})$. Its width is close to that of the tank, and it includes fluid heights between the grid's top position and the free surface. The cameras used are double frame LaVision sCmos sensors of 2560 by 2160 pixels, equipped with a 50 mm focal Macro lens. A pulsed Quantel Nd:YAG laser emitting at λ = 532 nm is used to illuminate 50 μm diameter polyamide particles. The collimated laser sheet thickness achieved is 200 μm. It is estimated by marking a photosensitive paper band placed on the wall of the tank closer to the laser head with a single laser pulse.

Depending on polymer concentration, the order of magnitude of measured velocities may differ considerably. In order to keep the measured particle displacement of the order of one third of the interrogation window, two types of PIV are used: double frame PIV for $C_{XG} < 250$ ppm, and single frame PIV for $C_{XG} \geq 250$ ppm. In the first case, the acquisition frequency f_{acq} is 4 Hz, and the time interval between laser pulses is Δt = 18 ms. In the second case, f_{acq} = 10 Hz, and consequently, Δt = 100 ms. Vector fields are computed with DaVis 8 software using a multipass processing: a first pass with 64 by 64 pixels and 2 following passes with 32 by 32 pixels round Gaussian weighted interrogation windows, at a maximum 50% overlap. Spurious vectors are removed from PIV fields by applying a threshold of 1.2 on the peak ratio and replaced using median filtering (always less than 10% of the total number of vectors).

The final spatial resolution achieved is 2.3 mm. The smallest Kolmogorov length scale and Taylor microscales of turbulence are supposed to be found in the water case, for which the viscosity is always the lowest. Based on the velocity and length scales, order of magnitudes shown in Figs. 7 and 9 (scales arbitrarily taken at z = 20 mm), Kolmogorov and Taylor length scales are evaluated to be, respectively, of about 0.19 mm and 2.24 mm. For 100 ppm XG solutions, using a constant viscosity equal to μ_∞, they increase to 0.33 mm and 3.25 mm, and up to 4.35 mm and 18.17 mm when using μ_0 as the scale viscosity. The 2.3 mm spatial resolution is thus quite coarse and would unfortunately not allow to evidence energy variations at large wave numbers characteristic of high Reynolds number viscoelastic turbulence. Yet, it is sufficient to discuss the large scale effects.

1000 vector fields are recorded for each run, corresponding to a measurement time of 250 s at f_{acq} = 4 Hz and 100 s at f_{acq} = 10 Hz. Assuming the integral time scale of turbulence to be of the order of magnitude of the grid period (this hypothesis could be checked for water and dilute regime XG solutions), this ensures a statistical analysis over at least 100 uncorrelated events. Each experiment is moreover performed twice.

In order to check for statistical convergence and estimate uncertainty on velocities, sliding statistics on 500 subsequent snapshots (time interval equal to $1/f_{acq}$) are computed for both experiments. For mean velocities and rms of velocity fluctuations, uncertainties are then estimated as the standard deviation of the variations of these samples' statistics around the "statistically converged" result obtained using the full data range. Typical velocity uncertainties thus evaluated are ±6% and ±5% for mean and rms quantities, respectively (spatial average on the whole ROI). Statistical convergence is ensured up to the previous confidence intervals.

IV. RESULTS

A. Mean flows and recirculations

1. Topology of the mean flow

The existence of mean flows and recirculations is most of the time an unwanted feature of OGT, which was initially meant to study

Published under license by AIP Publishing

turbulence alone in the absence of mean shear,[4] but can unfortunately not be avoided. They are supposedly due to the grid tendency to drift out of alignment and to initial minor fluid motion favoring the development of large scale motion and allowing mean flow patterns to persist once developed.[77] In the ROI, the mean flow is structured in two main recirculation vortices close to the grid and near the walls. Figure 3 shows in three columns, respectively, the average velocity field magnitude $\sqrt{\overline{U}_x^2 + \overline{U}_z^2}$ (with $\overline{U}_x$ and $\overline{U}_z$, respectively, the horizontal and vertical mean flow components), the associated streamlines, and the vorticity of the average velocity field $\overline{\Omega} = \nabla \wedge \overline{\mathbf{U}}$. These quantities are represented for water (first line) and three polymer concentrations: one in the dilute regime (10 ppm, second line), one in the semidilute regime (500 ppm last line) and one in the transition region (100 ppm, third line). The recirculation patterns observed on the streamline figures (central column) are evidenced by two opposite sign high magnitude vorticity patches on both sides of the tank, just above the grid sweep zone (right column). Isovalue lines of vorticity are drawn at the arbitrary threshold $\overline{\Omega} = \pm 0.02\overline{\Omega}_m$ with $\overline{\Omega}_m$ as the maximum vorticity value at a given concentration defined Sec. IV A 2. They represent an arbitrary estimation of the boundaries of the mean flow vortices. Similar flow patterns have also been observed by McKenna and McGillis[13] for water.

Based on the observation of Fig. 3 and additional intermediate concentrations (18, 25, 35, 50, 75, 150, and 250 ppm, not shown in the figure), the effect of polymer addition on the mean flow seems to be the following. When adding polymer to water, the flow organizes into two main regions dominated by the two counter rotative side vortices illustrated by the streamlines or the vorticity isovalues. Increasing polymer concentration first causes the mean flow vortices to grow in size until they reach the top of the fluid volume, at a concentration between 10 and 25 ppm. The flow is then divided into two main regions separated by a global up-going region at the center of the plane for concentrations between 25 and 100 ppm, as seen on Fig. 3, left and central columns. A further increase in concentration leads to the collapse of these recirculating regions: their size reduces (Fig. 3 central and right columns), and the central up-flowing region progressively disappears. Hypothesis will later be made on the probable reasons for this higher concentration behavior.

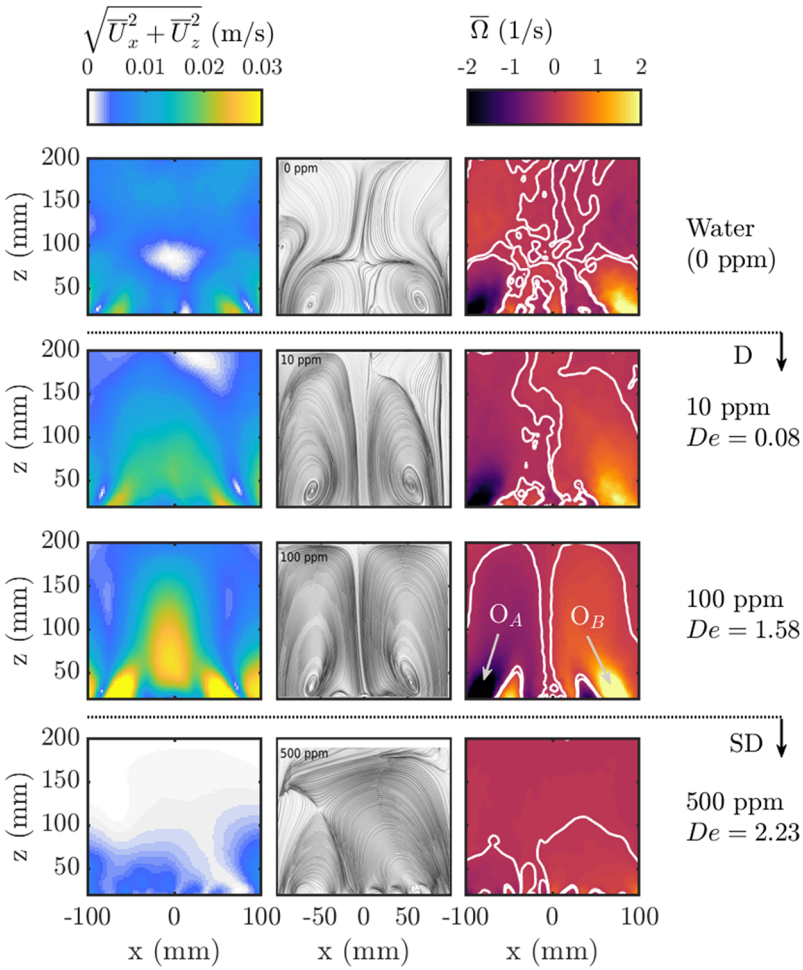

FIG. 3. Mean flow inside the grid stirred tank at different XG concentrations. Left column: norm of the 2D mean velocity field $\sqrt{\overline{U}_x^2 + \overline{U}_z^2}$ in m/s. Central columns: streamlines of the mean flow. Right column: Vorticity of the mean velocity field $\overline{\Omega} = \nabla \wedge \overline{\mathbf{U}}$, with contour lines drawn at 2% of the maximum vorticity value.

Published under license by AIP Publishing

2. Mean flow indicators

Simple indicators can be defined in order to measure the intensity and region of influence of the mean flow, and quantify the mean flow enhancement.

- The first criterion is the value of the curl of the average velocity field at the center of the side vortices. This is a measurement of the maximum vorticity in the mean flow, and thus, of the intensity of the side eddies. Here, it is defined as $\overline{\Omega}_m = max(\overline{\Omega}(O_A), \overline{\Omega}(O_B))$, where O_A is the central point of the left vortex and O_B the central point of the right vortex (see Fig. 3, right column). A nondimensional vorticity indicator can be constructed, multiplying $\overline{\Omega}$ by the polymer time scale t_{CY}.
- The second indicator is the peak-to-peak amplitude A (difference between maximum and minimum value) of the horizontal profile (along x) for the vertical component, $\overline{U}_z(x, z = Z_p)$, taken at a given probing altitude Z_p on the fields illustrated Fig. 3, left column. It is also a measurement of the intensity of the mean flow, but this time associated with the up-going motion. Here, we take $Z_p = 2M = 70$ mm, but a similar trend than the one presented hereinafter is observed for different Z_p. This velocity amplitude can be scaled by a grid based reference velocity: the product $f \times S$.
- The last indicator defined here is the position along z of the maximum vertical velocity on the $x = 0$ line (regardless of the value of this velocity). This is an estimation of the area of influence of the mean flow rather than of its intensity and comes as a complement of the two other indicators. It can be further normalized by the mesh parameter M.

The evolution of the peak vorticity magnitude with concentration (indicator 1) is shown in Fig. 4 and Table II. It increases with polymer concentration in the [0–150] ppm range and brutally decreases for the last two points. The critical concentration above which vortex intensity stops increasing, here 150 ppm, can be related to the transition concentration between the dilute and semidilute regime, 100 ppm. In the dilute regime, increasing polymer concentration and consequently the solution typical response time leads to an increase in maximum vorticity. When reaching the semidilute regime, further increase in concentration on the contrary reduces vorticity associated with mean recirculations. These observations are consistent with the streamline patterns observed in Fig. 3, central column: well defined structures build up upon polymer addition and grow in the dilute regime, and collapse between 100 and 500 ppm.

In the dilute regime, the characteristic time scale depends on concentration with the scaling $t_{CY} \sim C_{XG}^{1.5}$ (see Fig. 1). Since here $T = 1/f = 1$ s, scaling based on t_{CY} or De are equivalent. The dimensionless quantity $\overline{\Omega} t_{CY}$ is represented as a function of De [Fig. 4(b)]. It follows a power law such that $\overline{\Omega} t_{CY} \sim De^{1.39}$. Since here $t_{CY} \sim De$ [Eq. (5)], it implies that $\overline{\Omega} \sim De^{0.39}$. It should be mentioned that because of the limited range of time scales achievable in the dilute regime (difficulty of making polymer solutions at $C_{XG} < 10$ ppm) and of the single grid frequency used, this scaling is derived from a limited range of De. Larger variations of the Deborah number could be achieved by varying the grid frequency. Yet in the available range, the correlation is quite good. The intensity of mean recirculations increases with the solution time scale, but this increasing rate is reduced as the Deborah number increases (exponent below 1). Mean flow enhancement by polymer addition thus seems to be a low-concentration effect that loses efficiency approaching the semidilute regime. This may be explained by the fact that as the relaxation time increases with polymer concentration, viscosity also does. In the dilute regime, the zero shear rate viscosity scales as $C_{XG}^{1.6}$ [from Fig. 1(b)]; hence, it increases more rapidly than the relaxation time scale. In the semidilute regime, viscosity keeps increasing with the same trend but t_{CY} stays constant (note that Wyatt and Liberatore[76] observed a change of slope for the semidilute regime that is not observed here since no C_{XG} value is used in this domain). In that sense, it may be assumed that viscosity and time scale increase would have two different and maybe opposite effects on mean flows: the increase of the solution's time scale seems to enhance recirculations, whereas increasing viscosity tends to dissipate the flow structures and ultimately make them collapse.

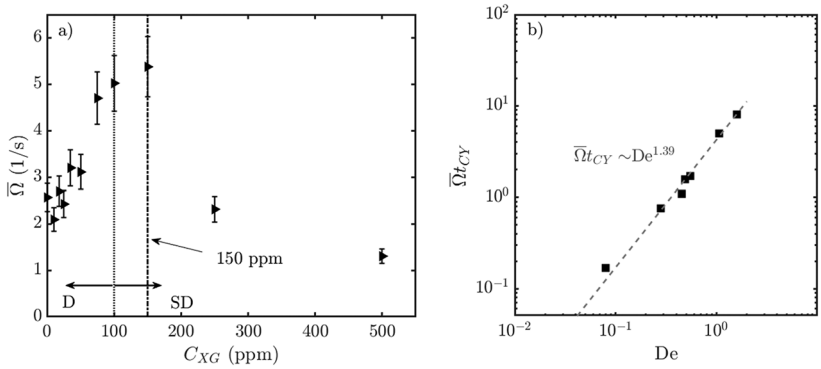

FIG. 4. Evolution of vorticity "strength" associated with mean flow structures as a function of polymer concentration and Deborah number. (a) is the maximum vorticity $\overline{\Omega}$ between the two counter-rotatives vortex plotted for all concentrations. The relative uncertainty is estimated to be less than ±12%, coming from the uncertainties on velocity measurement and from the spatial uncertainty on the location of O_A and O_B. (b) shows the nondimensional quantity $\overline{\Omega} t_{CY}$ in the extended dilute regime [$C_{XG} \leq 100$ ppm left of dashed dotted line in (a)]. The dotted line in (a) denotes the transition between dilute (D) and semidilute (SD) concentration regimes, and the dashed dotted marks line in (a) the change in trend at $C_{XG} = 150$ ppm. The gray dashed line in (b) is the power law fitting of $\overline{\Omega} t_{CY}$ vs De, the scaling of which is reported in (b) on top of the curve.

Published under license by AIP Publishing

A similar trend is observed when looking at the evolution of the second criterion with polymer concentration: the peak-to peak amplitude A of the horizontal profile for the vertical velocity component, probed at $z = Zp = 2M$, $\overline{U}_z(x, 2M)$. Figure 5(a) shows that polymer addition tends to promote a central up-going effect: the $\overline{U}_z(x, 2M)$ black dotted curve for water does not have its maximum value close to $x = 0$ mm, while it is the case for every polymer solutions at any concentrations. This peak effect is increased with polymer concentration until it reaches its maximum for $C_{XG} = 100$ ppm. The indicator A is defined as the curves' "peak-to-peak amplitude," that is to say the difference between the maximum and the minimum values of $\overline{U}_z(x, 2M)$ along x, sketched by the dashed arrow on Fig. 5(a). It is plotted as a function of the polymer concentration in Fig. 5(c). An increase compared to the water case is observed for all polymer solutions in the dilute regime. Indicator A seems to slightly increase with De within this dilute regime, even though the error bars on the data are also compatible with a constant A trend. It then collapses in the semidilute regime. This confirms that the intensity of the up-going central motion and that of the side vortices are coupled and that they are both related to the polymer entanglement concentration regime.

The third indicator is illustrated by Figs. 5(b) and 5(d). The vertical profiles of vertical velocity at $x = 0$ mm plotted in Fig. 5(b) all present a maximum value at small z (close to the grid). Yet, the $z = Z_m$ location of this maximum varies with polymer concentration. This can also be observed on the average velocity fields in Fig. 3, left column, and is a consequence of the flow organization into two side vortices. The impact region of both vortex meet in the plane of symmetry ($X = 0$ mm). Since the vortex is ellipsoidal and that their main axis is neither vertical nor horizontal, the maximum vertical velocity is found at a given altitude which depends on the inclination of the vortices and their topology. This third criterion thus evaluates the vortex pair's spatial influence more than their intensity. The altitude at which maximal vertical velocity is found Z_m is plotted vs concentration in Fig. 5(d). It shows an increasing trend in the early part of the dilute regime. However, unlike the up-going intensity A, it begins to decrease at a lower typical concentration, around 35 or 50 ppm.

Scaled second and third indicators can be plotted vs the Deborah number in the dilute regime. The evolution of A scaled by a reference grid velocity fS is shown in Fig. 5(e) and that of Z_m scaled by the mesh parameter M in Fig. 5(f), both in log-log scales. The first plot shows that as for $\overline{\Omega}t_{CY}$, $A/(fS)$ increases with the Deborah number, but on a very limited range. Figure 5(f) seems to confirm the existence of a critical concentration within the dilute regime: a peak of Z_m/M is observed precisely at $De = 0.55$ corresponding to

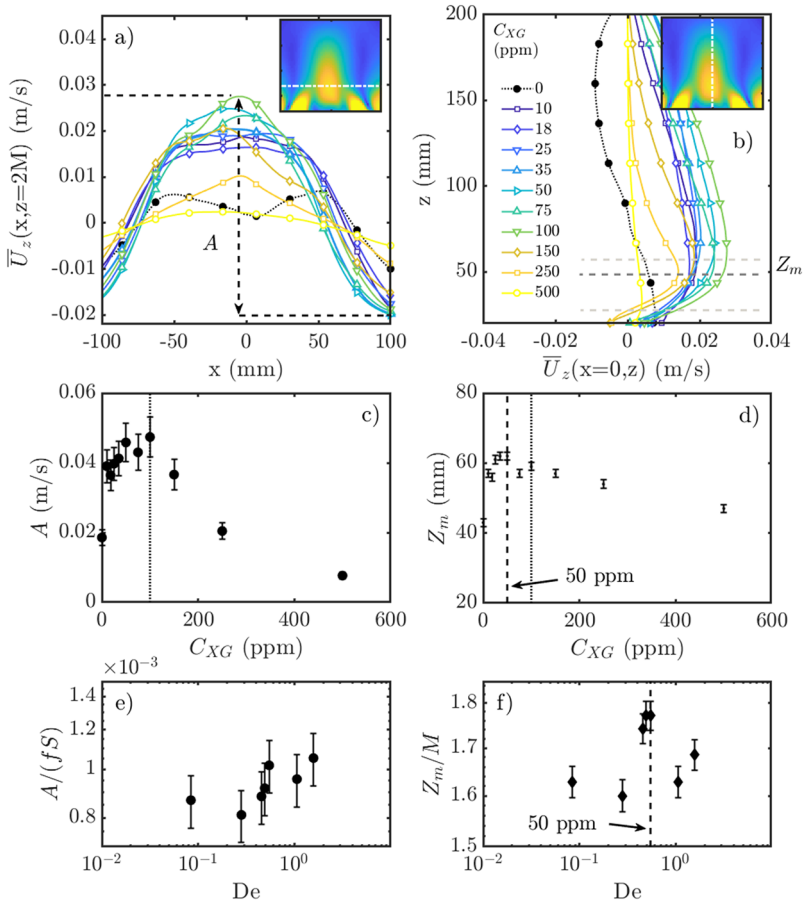

FIG. 5. Effect of polymer concentration on vertical velocity. (a) Horizontal profiles of the vertical velocity at $z = 2M = 70$ mm. Horizontal dashed lines and the vertical dashed arrow illustrate the peak-to-peak amplitude A indicator. (b) Vertical profiles of the vertical velocity at $x = 0$ mm. Gray horizontal dashed lines are examples of $z = Z_m$ depths for profile maxima. Inserts in (a) and (b) sketch the line along which profiles are plotted by a white dashed line, taking as an example the $C_{XG} = 100$ ppm average velocity field magnitude. Markers in (a) and (b) are represented for only one in ten data points, for the sake of readability. (c) Peak-to-peak amplitude A of the profiles of (a). (d) location Z_m along z of the maxima of profiles (b) (marker size is reduced so that the error bar can be seen). (e) and (f) show the evolution with De in the dilute regime of the two previous indicators, respectively A and Z_m, scaled by, respectively, fS and M (in log scale). The dotted lines in (c) and (d) denote the dilute to semidilute entanglement transition ($C_{XG} = 100$ ppm). The black dashed line in (d) and (f) corresponds to the subdilute critical concentration $C_{XG} = 50$ ppm.

Published under license by AIP Publishing

C_{XG} = 50 ppm, even if the relative variations of Z_m/M are quite small in the studied *De* range.

One can quickly comment on the uncertainties of the plots in Fig. 5. In (a) and (b), the relative uncertainty on velocity value along these profiles is typically equivalent to that on mean velocity, i.e., about ±6%. Hence the relative uncertainty on A and $A/(fS)$ is twice that value, about ±12%. The absolute uncertainty on Z_m points in (d) would be evaluated as ± 1.15 mm (from the PIV spatial resolution), which gives a relative uncertainty on Z_m and Z_m/M less than 3%.

The effects of polymer addition and polymer concentration on mean flows inside the tank can thus be summarized as follows:

- Polymer addition has an organizing effect on the mean flow. Existing vortices are enhanced by addition of even a small concentration of polymer, and the flow organizes into two distinct vorticity regions ruled by the pair of counter rotative eddies. A global up-going motion appears at the center of the tank.
- Increasing polymer concentration while staying in the dilute regime tends to increase the vortex and up-going motion intensity. Both indicators for vortex and up-going motion intensity increase until concentration reaches the critical concentration C_{XG} = 100 ppm for which solution switches from dilute to semidilute regimes. In the concentration range corresponding to the dilute regime, the maximum vorticity of the mean flow scales as a power law of the Deborah number.
- The region of influence of the mean flow is observed to increase at the onset of polymer addition, but the maximum effect of the up-going motion is attained at a concentration lower than the dilute to semidilute transition. This suggests that the dilute regime is itself composed of two subregimes: a very dilute one in which both vortex intensity and size increase, and a transition to semidilute one in which the vortex intensity keeps increasing but its region of influence reduces.
- In the semidilute domain, vortex intensity and size both decrease. The hypothesis is that in this regime, viscosity keeps increasing upon polymer addition while elasticity of the polymer chains is limited because of emerging polymer-polymer interactions.

B. Turbulence properties

Turbulence properties are evaluated in the central region of the ROI, where they are the most homogeneous[42] by cropping out bands for $x > 2.5M$ and $x < -2.5M$ on the sides of the ROI before width averaging quantities (along x) and plotting vertical profiles (along z). This central region is illustrated in Fig. 6 where two examples (water and 25 ppm XG) of turbulent kinetic energy fields k, computed as $k = u_z'^2 + 2u_x'^2$, are shown in log scale. Note that the kinetic energy is computed under an assumption of horizontal isotropy. In the following analysis, all profiles are plotted vs the unscaled dimension z in order to compare with dimensional HT and TT relationships for OGT [Eqs. (1) and (2)].

1. Decay of turbulence intensity

Profiles of u_x' as a function of z are shown in Fig. 7(a). For C_{XG} < 250 ppm, it appears that all the profiles, water and polymer solutions, follow a power law of constant exponent as predicted by the relationship of Hopfinger and Toly[4] [Eqs. (1)]. The first important observation is thus that the decay of turbulence intensity of OGT in the dilute regime of polymer solutions can be described by "HT-like" profiles. The influence of polymer concentration on this decay is quantified by the power law exponent. In the picture of Hopfinger and Toly,[4] u_x' and u_z' should be proportional, resulting in a single value of n. Following this hypothesis, this value is estimated for each concentration by fitting both the u_x' and u_z' (not shown here) profiles with power laws, and averaging the two resulting exponents. The difference between these two exponents yields the dispersion bars represented on Fig. 7 (corresponding to the uncertainties in Table II).

Values of n are reported in Table II and plotted vs concentration in Fig. 7(b) (for the whole C_{XG} < 250 ppm range) and (c) (zoomed on C_{XG} < 100 ppm). It appears that the n value for water is slightly above the n = −1 expected from HT. When adding polymer n starts increasing up to −0.716 at 18 ppm [Fig. 7(c)] before decreasing again, quasilinearly with polymer concentration, until C_{XG} = 150 ppm, where it is equal n = −1.479. The decay rate of oscillating grid turbulence thus varies with polymer concentration, staying quite similar to the water case as long as one stays in the dilute regime.

In the semidilute regime, the decay of turbulence departs from the HT behavior: the last two concentrations exhibit two asymptotic slopes separated by a transition area, a first one n', at small z, which keeps decreasing with increasing C_{XG} but not following the linear trend of n, and a second one n'' = 0 at large z. In this second region, turbulent velocity fluctuations are extremely small and the mean flow is low as well (see Fig. 3). Viscous dissipation reduces the velocity magnitudes, hence the local shear rate, which further increases viscosity and consequently the dissipation (negative n). This accumulated effect makes the fluid practically turbulence-free

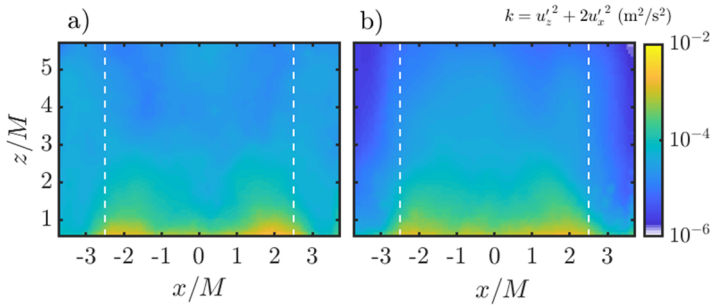

FIG. 6. Fields of turbulent kinetic energy $k = u_z'^2 + 2u_x'^2$ in log scale for water (a) and 25 ppm XG solution (b). Vertical dashed lines at x/M = ±2.5 denote the boundaries of the domain for horizontally averaged turbulence properties.

Published under license by AIP Publishing

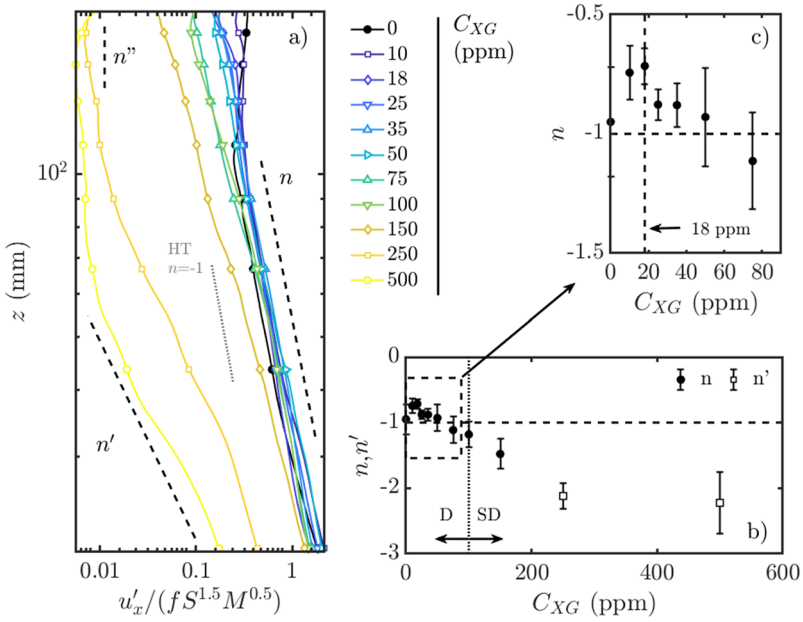

FIG. 7. "HT-like" plots of u'_x as a function of z (a) and estimation of the power law exponent evolution as a function of polymer concentration (b). (c) is a zoom of (b) in the C_{XG} < 100 ppm range. Markers in (a) are represented for only one in ten data points, for the sake of readability. The typical uncertainty on u'_x is ±5%. Vertical bars in (b) and (c) show the disparity of n measurement from u'_x and u'_z profiles.

and motionless, which is in some ways equivalent to a cavern effect observed in stirred tanks.[78]

2. Mean flow to turbulence ratio

A key quantity of oscillating grid turbulence is the local mean to turbulence ratio $\Gamma_{ij} = \frac{|\overline{U}_i|}{u'_j}$, between the local absolute value of mean velocity component $|\overline{U}_i|$ and the local rms of turbulent velocity fluctuations component u'_j, with i = x, y, or z. Γ_{ij} is a 9 component tensor, which reduces to a 4 component tensor with $i, j = x$ or z for 2D PIV measurements. Most of the time, the values used to estimate the efficiency of a device in terms of turbulence vs mean flow production are diagonal values Γ_{ii}. Here, we compute the indicator Γ as the width average of the quantity $\left(\sum_i \Gamma_{ii}^2\right)^{0.5}$. For OGT in water, a review by Variano, Bodenschatz, and Cowen[77] reports local typical best case values of $\Gamma_{ii} = 0.25$ in a single coordinate direction. Here, Fig. 8 shows that width averaged Γ lies between 0.9 and 3.5 for all fluids. Yet, it has to be mentioned that mean flow over turbulence ratio can locally reach higher values of up to 10 in the central region where the mean flow is very strong, and down to 0.1 in high turbulence intensity/low mean flow regions. Γ globally increases with polymer concentration, which is a consequence of both the enhancement of the mean flow and the decrease of turbulence intensity. Three distinct regions can be seen on the plot of Γ vs z. The first one (1), for $z < M$ and in which $\Gamma < 2$, lays just below the main mean flow structure detailed previously. The second one (2) between $z = M$ and $z = 4M$ corresponds to the region of the up-going motion and side recirculations and yields the highest Γ values going along with the strongest mean flows. In regions (1) and (2), Γ is always the lowest for water. The third region (3) corresponds to the distances not reached by the principal mean flow structure in polymer solutions, or in which their intensity is reduced, but where turbulence keeps decaying. The values of Γ in the far grid region (3) depend on the existence or not of secondary recirculations under the free surface. They are comparable to those found for water and can even be lower than in water in some dilute polymer solutions. In region (3), mean flow intensity is at worst twice that of turbulence, no matter the working fluid.

3. Integral length scales

The integral length scales of turbulence L_{ij}^k are defined as the integral of correlation coefficients of velocity fluctuation components i and j along dimension k, with i, j or $k = x$ or z. They are averaged over sampling regions at different depths. Length scales along x are computed on sampling regions wide as the ROI and including 3 vectors in the z direction. Length scales along z are

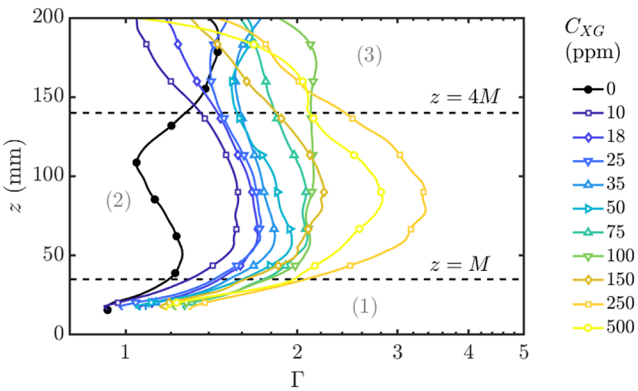

FIG. 8. Plots of the mean flow to turbulence indicator Γ, in log scale, as a function of the distance from the grid z. Dashed lines are plotted at $z = M$ and $z = 4M$. Markers are represented for only one in ten data points, for the sake of readability. The typical uncertainty on Γ is ±11%, sum of the uncertainties on $\overline{U}$ ans u'_x.

Published under license by AIP Publishing

computed on sampling regions of width equal to that of the ROI's and 10 mm height. The study of integral scales is limited to the dilute regime. As for mean and rms velocities, uncertainties are estimated by computing sliding statistics on 500 images samples and evaluating the variations of the integral length scales computed from these samples around the converged value derived from the full data range. This yields a typical uncertainty of ±10% on horizontal scales L^x_{xx} and of ±12% on vertical scales L^z_{zz}.

In the definition of Thompson and Turner,[3] L is equal to the horizontal scale of horizontal velocity fluctuations L^x_{xx}. Figure 9 shows the evolution of $L = L^x_{xx}$ (a) and of the vertical scale of vertical velocity fluctuations L^z_{zz} (b) as a function of the distance to the grid z. Integral scales are larger in polymer solutions compared to water. This was previously observed in several studies of turbulence in shear-thinning or viscoelastic polymer solutions.[56,59,60]

It appears that up to a given proximity of the free surface, which is located at $z = 250$ mm, both L^x_{xx} and L^z_{zz} scales follow a linear trend with z, as observed by Thompson and Turner[3] in water. We notice that the change in trend trend happens at higher depths (smaller z) for the vertical scale L^z_{zz} than for the horizontal one and that this depths increases with polymer concentration. This is consistent with the fact that vertical velocity structures are kinematically constrained by the horizontal interface, and larger for large polymer concentrations (to be detailed in Lacassagne *et al.*[79]).

As for the slope of the different linear trends, denoted, respectively, α for L^x_{xx} and β for L^z_{zz}, they are reported in the subfigure (c) of Fig. 9 and compared with the value predicted by Thompson and Turner[3] for water, $C_{TT} = 0.1$. The value of α for $C_{XG} = 0$ is quite close to the expected C_{TT} value. Both α and β increase with polymer concentration up to 50 ppm and seem to initiate a decrease for $C_{XG} > 50$ ppm, meaning that the growth of flow structure moving away from the grid is enhanced by the presence of polymer at the onset of the dilute regime and that this enhancement may no longer happen in the semidilute one.

Finally, the relative evolution of L^z_{zz} and L^x_{xx} can be quantified by computing the ratio $r = \beta/\alpha$ at each concentration. $r > 1$ indicates that the vertical dimension of structures increases faster that the horizontal one, and $r < 1$ the opposite. Figure 9(d) shows that r is slightly below 1 for water, but increases up to a value of almost 2 for $C_{XG} = 50$ ppm before decreasing again for $C_{XG} = 100$ ppm. The conclusion to that is that the presence of polymer in the concentration range $C_{XG} \leq 50$ ppm not only enhances the growth of turbulence structures moving away from the grid but also the anisotropy of the growth: the vertical elongation of eddies is promoted. Both behavior yet seem to reduce when approaching the semidilute regime.

4. Isotropy

For OGT in water, it is known that the vertical component of turbulence is stronger than the horizontal one because this is the orientation of the grid forcing. Hence, OGT is by nature not fully isotropic in a vertical plane. An indicator of the 2D isotropy of turbulence in the $(\vec{x}, \vec{z})$ plane, I_s, can be defined by dividing the HT profiles of the vertical component by the horizontal one, $I_s = u'_z/u'_x$.

The I_s indicator is as expected generally above 1, thus confirming that the vertical velocity fluctuations rms is always larger than the horizontal one, for water and all polymer concentrations. According to the description of Hopfinger and Toly,[4] the rms of vertical velocity fluctuations should be proportional to the rms of horizontal ones with a constant proportionality coefficient C_{2HT}. I_s profiles should thus be constant along z, which is here only observed as a first approximation in the dilute regime as will be discussed hereinafter. In this first approximation, the anisotropy coefficient, corresponding to the second HT constant C_{2HT}, can then be obtained for each working fluid as the average of I_s over z (Fig. 10). In the literature (see Sec. II A 1), its value is between 1.1 and 1.4 for water.

C_{2HT} is found to increase with polymer concentration (see Fig. 10 and values reported in Table II), first moderately, and then

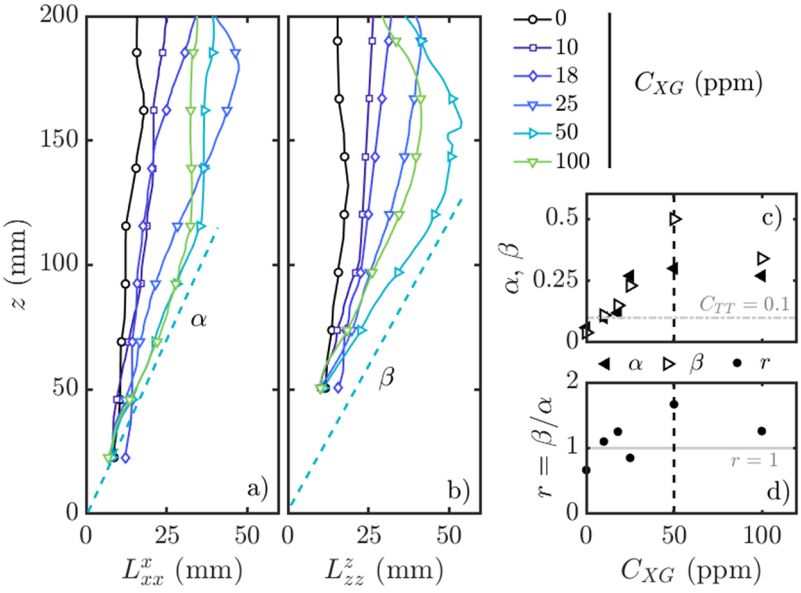

FIG. 9. Integral length scales of turbulence in the dilute regime. (a) Horizontal scale of horizontal velocity fluctuations L^x_{xx} as a function of the distance to the grid z. (b) Vertical scale of vertical velocity fluctuations L^z_{zz} as a function of the distance to the grid z. Markers in (a) and (b) are represented for only one in ten data points, for the sake of readability. (c) Slopes α and β of linear trends of, respectively, L^x_{xx} and L^z_{zz} a small z, as a function of polymer concentration. (d) Ratio of these two slopes $r = \beta/\alpha$.

Published under license by AIP Publishing

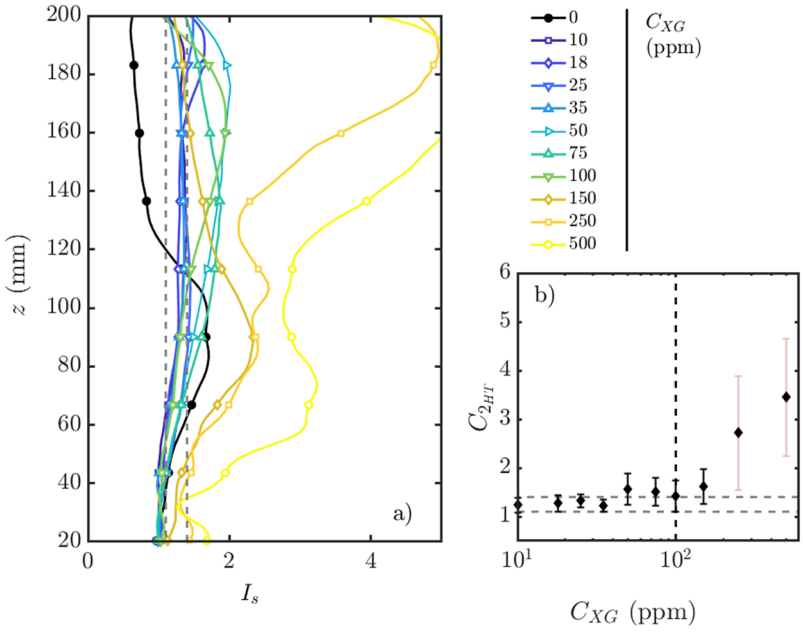

FIG. 10. Vertical profiles of anisotropy I_s for water and polymer solutions at different concentrations. (a) I_s Isotropy profiles. The typical uncertainty on I_s is twice that of u'_x or u'_z profiles, i.e., ±10%. (b) Evolution of $C_{2_{HT}}$, computed as the average of I_s over z, with polymer concentration. Dashed lines are boundaries of the usual range of values found in water $1.1 < C_{2_{HT}} < 1.4$. Vertical bars represent standard deviation of $C_{2_{HT}}$ along z around its average value for each concentration. Markers in (a) are represented for only one in ten data points, for the sake of readability.

faster above 100 ppm concentrations. The first conclusion is thus that the presence of polymer tends to promote turbulence anisotropy and that this increased anisotropy is all the more important when polymer concentration is high. Yet, for concentrations lower than 100 ppm, the value of HT's second constant stay inside the range found in the literature for water up to the error bar amplitude, despite the slight increase observed. When entering the semidilute regime, that is to say at concentrations above 100 ppm, C_{2HT} increases much faster with concentration.

Nevertheless, looking at the evolution of I_s with z, we notice that for polymer solutions, a slight increase of I_s is observed with increasing z. Barely visible at low concentrations, this increase seems all the more important that polymer concentration is high, especially for $C_{XG} \geq 250$ ppm. For the two higher concentrations studied, I_s is clearly no longer constant with z. The estimation of $C_{2_{HT}}$ by z-averaging of I_s should thus be interpreted carefully: as long as I_s can be considered constant with z, here to a first approach for $C_{XG} \leq 100$ ppm, the hypothesis of HT holds and anisotropy can be fully described by the evolution of $C_{2_{HT}}$. When I_s increases with z, it means that u'_x and u'_z are no longer proportional and that u'_z increases faster than u'_x. Hence the HT exponent for u'_z is likely higher than the one for u'_x. Anisotropy is then expressed not only by $C_{2_{HT}}$ but also by the ratio of decay exponents for u'_x and u'_z. Increased anisotropy of turbulence in polymer solutions was already observed by Gupta, Sureshkumar, and Khomami[64] or Cai *et al.*[63] in channel flows of viscoelastic polymers, or in turbulent front propagation experiments by Cocconi *et al.*[57] In the first case, it is explained by the ability of polymer chains to align with the mean flow. In the second one, it likely comes from a reorganization of turbulence leading to an alignment of polymers with vorticity, which is, as the authors stress out, somehow similar to the mean-flow alignment observed in channel flows. Here, the fact that $C_{2_{HT}}$ is above unity and increases with C_{XG} fits well in this picture: the grid motion being vertical, polymer chains preferentially settle along the periodic vertical shear induced by the grid, and vertical turbulent fluctuations are promoted. The specific behavior observed in the semidilute regime has to be tempered by the fact that for such concentrations turbulence is very weak, event in the region close to the grid, and transitions to laminar or even motionless in the rest of the tank.

As a last remark, one notices that when approaching the free surface (located here at Z close to 250 mm), the previous increasing trend of I_s with z is reversed, the values of I_s decrease. This suggests that the free surface damps the vertical fluctuations of turbulence more efficiently than the horizontal ones (see Ref. 79). Not accounted for by the laws of Ref. 4, this could translate by a strong differentiation of the two power law exponents for u'_x and u'_z.

5. Homogeneity

Finally, in order to measure horizontal homogeneity, we define the quantity H_j^x as the standard deviation over an horizontal line at altitude z of the 2D field of rms velocity fluctuations in dimension j (j being x or z), normalized by the reference (width averaged) rms u'_j at this depth. The smaller the H_x^x or H_z^x, the higher the homogeneity in dimension x at a given z. Homogeneity indicators H_z^x or H_x^x do not show any trend along z. Values of H_z^x averaged over z, denoted H, are reported in Table II. Uncertainty on H value is computed as the standard deviation of H_z^x over z. H does not seem to depend on polymer concentration. This implies that polymer has a lesser effect on turbulence homogeneity than on its isotropy. This is obviously only valid in the central region of the ROI defined previously, for $-2.5M < x < 2.5M$.

Published under license by AIP Publishing

V. DISCUSSION

A. Concentration regimes and drag reduction

Several characteristic polymer concentrations emerge from the previous results and observations. The different concentration subranges and their characteristics in terms of mean flow and turbulence are summarized in Fig. 11. Apart from the 100 ppm concentration which marks the transition between the dilute and semidilute regime, two specific critical concentrations can be evidenced within the dilute regime itself: $C_{XG} = C_{D1} \simeq 20$ ppm and $C_{XG} = C_{D2} \simeq 50$ ppm. This leads to three dilute subregimes referred to as D0, D1 and D2.

The first critical concentration marks the limit of an extremely dilute behavior of the polymer corresponding D0 to the very onset of polymer action on both mean flows and turbulence. It is worth noting that the existence of such turbulent inner dilute regimes was already evidenced for other polymer molecules (PEO, with a 25 ppm critical concentration[29,80]).

The second one corresponds to the maximum mean flow enhancement concentration reached between D1 and D2 (all mean flow indicators increase between 0 and 50 ppm), and also to the maximum large turbulent scale enhancement, in an anisotropic fashion (see Fig. 9). It can be inferred that this state of maximize mean flow, found at 50 ppm, corresponds to a given state of polymer-flow interactions (alignment, ratios between polymer relaxation time scales and turbulent time scales. . .). A maximized mean flow would imply that interactions between polymer and small turbulent structures are reduced and energy transfer toward large scales of the flow are favored. The question is then the flowing: since the polymer concentration lies inside the dilute entanglement regime (lower than 100 ppm) for which mechanical interactions between polymer chains is assumed negligible, what then causes polymer chains to exhibit variable response to the flow? A possible explanation is the existence of polymer-polymer electrical interactions. It is indeed known that when transitioning from the dilute to the semidilute regime, long chained XG molecules first see each other through repulsive and attractive electrical forces caused by the presence of electrically charged complex on the polymer carbonate backbone.[76] Would this mean that the critical 50 ppm concentration marks the onset of polymer electrical interactions, "smoothing" the dilute to semidilute transition? This open question needs to be answered by a coupling between the knowledge of typical flow time scales, and theoretical models of polymer conformation state and electrical interactions.

It is in that sense interesting to notice that a critical concentration for drag reduction of XG solutions is found quite close, at $C_{XG} = 70$ ppm by Wyatt, Gunther, and Liberatore.[81] These previous concentrations can indeed be related to the drag reduction properties (type B) of XG. Wyatt, Gunther, and Liberatore[81] evidenced drag reduction for XG flowing in pipes at XG concentrations down to 20 ppm. Sohn *et al.*[82] achieved drag reduction by XG in a rotating disk apparatus at concentrations down to 10 ppm, but found a critical concentration for maximum drag reduction at 200 ppm. Pereira, Andrade, and Soares[83] observed drag reduction for XG concentration as low as 2 ppm, and a critical concentration at 37.5 ppm below which drag reduction efficiency falls with increasing C_{XG} and above which it increases. They stressed that this last two-trend behavior is significantly different from that of type A drag reducing polymers, for which drag reduction monotonously increases with polymer concentration. These last remarks support our observations that several hydrodynamic subregimes of concentration can exist for XG and long chained polymers. As it is the case for drag reducing properties, the values of these critical concentrations should depend on the conformation of the polymer chains, on the presence of salt that may modify this conformation,[84,85] on the entanglement state, and on the molecular weight of the polymer chains.[76,83] The first critical concentration C_{D1}, comparing to low critical drag reduction concentrations, is thus likely related to conformation effects and physical properties of polymer chains. The second, higher, critical concentration C_{D2} could be explainable by mean shear alignment effects. The critical concentration, $C_{XG} = 100$ ppm (and the 100 ppm–150 ppm transition) is by definition connected to polymer-polymer interactions.

B. Possible mean flow production and feeding mechanisms

In McCorquodale and Munro,[42] a physical explanation of the origin of the mean flow in OGT is proposed. The authors argue that mean flow arises when there is "*a significant difference in the relative strengths of the jets produced by the oscillating grid in different regions of the tank*," and relate it to a Coanda effect applying on the jets closer to the walls. The authors check that when artificially separating the side jets from the central ones, using an inner box, mean

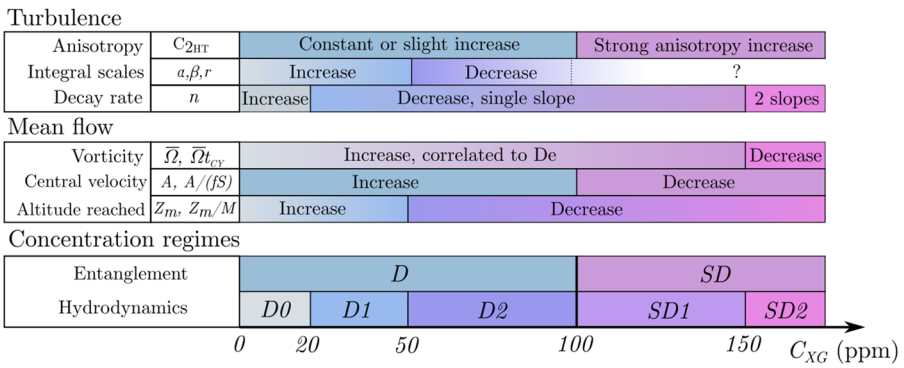

FIG. 11. Summary of indicators and flow properties evolution with concentration, and sketch of concentration regimes and subregimes.

Published under license by AIP Publishing

flow intensity is significantly reduced inside that inner box. What can be added to this picture when the working fluid is a shear thinning polymer solution, is the fact that strong shearing of the fluid in the region between the grid and the wall tends to locally reduce the average viscosity on the sides of the tank. Jets induced by the grid motion are thus by nature of even more variable strength depending on their distance from the wall: near wall jets on each side of the tank see a statistically lower viscosity than jets close to $x = 0$. The fact that mean flow is enhanced in the presence of polymer in the dilute regime is thus consistent with the mean flow origin proposed by McCorquodale and Munro.[42]

It has also been shown in several studies that the effect of polymer can propagate to larger scales (see Sec. II B). This can translate for example into an increase of integral length scales and of large scale fluctuations of velocity.[56,59,60] This up-scale energy transfer[55] could be another feeding mechanisms for the mean flow, explaining its enhancement with increasing polymer concentration in the dilute regime. To confirm such an hypothesis, it would be interesting to study turbulence inside the grid sweep region and try to evidence energy transfer terms that could fuel the mean flow.

VI. CONCLUSION AND PERSPECTIVES

In this work, the hydrodynamics in an oscillating grid stirred tank filled with either water or shear-thinning XG solutions have been investigated. It is found that the presence of polymer tends to enhance the mean flow in the dilute regime, by structuring and increasing the two side recirculations already existing in water. This mean flow increase can be related to the shear-thinning Deborah number in the dilute regime. In the semidilute regime, the further increase of viscosity not being followed by an increase in De leads to a collapse of the mean flow. As for turbulence, its properties also evolve with polymer concentration, especially its decay rate, its isotropy, and the size of its largest turbulent structures. In the dilute regime, the HT and TT descriptions of OGT in water can be adapted to shear thinning XG solutions.

Oscillating grid apparatuses can thus be used as tools to generate controlled turbulence in dilute regime shear thinning polymer solutions. In this concentration range, laws for OGT in dilute polymer solutions can be compared to those in water. A non-negligible mean flow has to be accounted for, but it is mostly acting in the bulk flow of OGT in the $z < 4M$ region. Mean flow over turbulent intensity levels remain comparable closer to the free surface for $z > 4M$, making it possible to study turbulence, mixing and mass transfer boundary layers in such fluids, as done in water.

The overall evolution of hydrodynamic properties with polymer concentration can be described by several critical concentrations, splitting the dilute and semidilute entanglement regimes into several hydrodynamic subregimes. In particular, it is worth noting that transition exists at concentrations as low as about $C_{XG} \simeq 20$ ppm, comparable to critical concentrations for drag reduction. A more extensive characterization of turbulence properties would come from a parametric study of the influence of f, S or M on the velocity and integral scales of turbulence. This could, for example, allow to discuss the value of $C_{1_{HT}}$ in polymer solutions, and its possible dependency on Re_g. Three-dimensional effects in turbulence and mean flow could be investigated by either additional PIV measurements in other planes of the tank or directly by using three-dimensional particle tracking methods. Finally, the mechanisms of turbulence and mean flow production at the grid level remain to be fully understood. Interesting data could be brought by velocity measurements inside the grid sweep region, and by the study of energy fluxes transferred between oscillating motion induced by the grid, turbulence, and mean flow structures.

REFERENCES

[1] M. W. McCorquodale and R. J. Munro, "Experimental study of oscillating-grid turbulence interacting with a solid boundary," J. Fluid Mech. **813**, 768–798 (2017).

[2] M. W. McCorquodale and R. J. Munro, "Analysis of intercomponent energy transfer in the interaction of oscillating-grid turbulence with an impermeable boundary," Phys. Fluids **30**, 015105 (2018).

[3] S. M. Thompson and J. S. Turner, "Mixing across an interface due to turbulence generated by an oscillating grid," J. Fluid Mech. **67**, 349–368 (1975).

[4] E. J. Hopfinger and J.-A. Toly, "Spatially decaying turbulence and its relation to mixing across density interfaces," J. Fluid Mech. **78**, 155–175 (1976).

[5] E. Xuequan and E. J. Hopfinger, "On mixing across an interface in stably stratified fluid," J. Fluid Mech. **166**, 227–244 (1986).

[6] L. Verso, M. van Reeuwijk, and A. Liberzon, "Steady state model and experiment for an oscillating grid turbulent two-layer stratified flow," Phys. Rev. Fluids **2**, 104605 (2017).

[7] Y. Nagami and T. Saito, "An experimental study of the modulation of the bubble motion by gas–liquid-phase interaction in oscillating-grid decaying turbulence," Flow, Turbul. Combust. **92**, 147–174 (2013).

[8] L. San, T. Long, and C. C. K. Liu, "Algal bioproductivity in turbulent water: An experimental study," Water **9**, 304 (2017).

[9] M. Rastello, H. Michallet, and J.-L. Marié, "Sediment erosion in zero-mean-shear turbulence," in *Coastal Dynamics* (2017), pp. 597–607; available at https://hal.archives-ouvertes.fr/hal-01626359/.

[10] M. T. Mahamod, W. H. M. W. Mohtar, and S. F. M. Yusoff, "Spatial and temporal behavior of Pb, Cd and Zn release during short term low intensity resuspension events," J. Teknol. **80**, 17–25 (2018).

[11] R. Vonlanthen and P. A. Monkewitz, "Grid turbulence in dilute polymer solutions: PEO in water," J. Fluid Mech. **730**, 76–98 (2013).

[12] B. H. Brumley and G. H. Jirka, "Near-surface turbulence in a grid-stirred tank," J. Fluid Mech. **183**, 235–263 (1987).

[13] S. P. McKenna and W. R. McGillis, "The role of free-surface turbulence and surfactants in air–water gas transfer," Int. J. Heat Mass Transfer **47**, 539–553 (2004).

[14] H. Herlina, "Gas transfer at the air-water interface in a turbulent flow environment," Ph.D. thesis, Universitätsverlag Karlsruhe, Karlsruhe, 2005.

[15] L. Chiapponi, S. Longo, and M. Tonelli, "Experimental study on oscillating grid turbulence and free surface fluctuation," Exp. Fluids **53**, 1515–1531 (2012).

[16] J. Magnaudet, "High-Reynolds-number turbulence in a shear-free boundary layer: Revisiting the Hunt–Graham theory," J. Fluid Mech. **484**, 167–196 (2003).

[17] J. Magnaudet and I. Calmet, "Turbulent mass transfer through a flat shear-free surface," J. Fluid Mech. **553**, 155–185 (2006).

[18] H. Herlina and J. G. Wissink, "Direct numerical simulation of turbulent scalar transport across a flat surface," J. Fluid Mech. **744**, 217–249 (2014).

[19] H. Herlina and G. H. Jirka, "Experiments on gas transfer at the air–water interface induced by oscillating grid turbulence," J. Fluid Mech. **594**, 183–208 (2008).

[20] J. G. Janzen, H. Herlina, G. H. Jirka, H. E. Schulz, and J. S. Gulliver, "Estimation of mass transfer velocity based on measured turbulence parameters," AIChE J. **56**, 2005–2017 (2010).

[21] D. E. Turney and S. Banerjee, "Air–water gas transfer and near-surface motions," J. Fluid Mech. **733**, 588–624 (2013).

Published under license by AIP Publishing

[22]E. A. Variano and E. A. Cowen, "Turbulent transport of a high-Schmidt-number scalar near an air–water interface," J. Fluid Mech. **731**, 259–287 (2013).
[23]T. Lacassagne, M. EL-Hajem, F. Morge, S. Simoëns, and J.-Y. Champagne, "Study of gas liquid mass transfer in a grid stirred tank," Oil Gas Sci. Technol. **72**, 7 (2017).
[24]H. Herlina and J. G. Wissink, "Isotropic-turbulence-induced mass transfer across a severely contaminated water surface," J. Fluid Mech. **797**, 665–682 (2016).
[25]J. G. Wissink, H. Herlina, Y. Akar, and M. Uhlmann, "Effect of surface contamination on interfacial mass transfer rate," J. Fluid Mech. **830**, 5–34 (2017).
[26]Y. Kawase, B. Halard, and M. Moo-Young, "Theoretical prediction of volumetric mass transfer coefficients in bubble columns for Newtonian and non-Newtonian fluids," Chem. Eng. Sci. **42**, 1609–1617 (1987).
[27]M. Jimenez, N. Dietrich, J. R. Grace, and G. Hébrard, "Oxygen mass transfer and hydrodynamic behaviour in wastewater: Determination of local impact of surfactants by visualization techniques," Water Res. **58**, 111–121 (2014).
[28]A. de Lamotte, A. Delafosse, S. Calvo, F. Delvigne, and D. Toye, "Investigating the effects of hydrodynamics and mixing on mass transfer through the free-surface in stirred tank bioreactors," Chem. Eng. Sci. **172**, 125–142 (2017).
[29]A. Liberzon, M. Holzner, B. Lüthi, M. Guala, and W. Kinzelbach, "On turbulent entrainment and dissipation in dilute polymer solutions," Phys. Fluids **21**, 035107 (2009).
[30]Y. Wang, W.-H. Cai, T.-Z. Wei, L. Wang, and F.-C. Li, *Experimental Study on Two-Oscillating Grid Turbulence with Polymer Additives* (ASME, Seoul, South Korea, 2015), p. V001T15A008.
[31]Y. Wang, W.-H. Cai, T.-Z. Wei, H.-N. Zhang, L. Wang, and F.-C. Li, "Proper orthogonal decomposition analysis for two-oscillating grid turbulence with viscoelastic fluids," Adv. Mech. Eng. **8**, 1687814016679773 (2016).
[32]S. I. Voropayev and H. J. S. Fernando, "Propagation of grid turbulence in homogeneous fluids," Phys. Fluids **8**, 2435–2440 (1996).
[33]H. J. Rouse and J. Dodu, "Turbulent diffusion across a density discontinuity," La Houille Blanche **4**, 522–532 (1955).
[34]M. Bouvard and H. Dumas, "Application de la méthode de fil chaud à la mesure de la turbulence dans l'eau," La Houille Blanche **3**, 257–270 (1967).
[35]T. J. Mcdougall, "Measurements of turbulence in a zero-mean-shear mixed layer," J. Fluid Mech. **94**, 409–431 (1979).
[36]R. I. Nokes, "On the entrainment rate across a density interface," J. Fluid Mech. **188**, 185–204 (1988).
[37]I. P. D. De Silva and H. J. S. Fernando, "Some aspects of mixing in a stratified turbulent patch," J. Fluid Mech. **240**, 601–625 (1992).
[38]C. R. Chu and G. H. Jirka, "Turbulent gas flux measurements below the air-water interface of a grid-stirred tank," Int. J. Heat Mass Transfer **35**, 1957–1968 (1992).
[39]N. Matsunaga, Y. Sugihara, T. Komatsu, and A. Masuda, "Quantitative properties of oscillating-grid turbulence in a homogeneous fluid," Fluid Dyn. Res. **25**, 147–165 (1999).
[40]W. H. M. Wan Mohtar, "Oscillating-grid turbulence at large strokes: Revisiting the equation of Hopfinger and Toly," J. Hydrodyn. **28**, 473–481 (2016).
[41]S. P. McKenna and W. R. McGillis, "Observations of flow repeatability and secondary circulation in an oscillating grid-stirred tank," Phys. Fluids **16**, 3499–3502 (2004).
[42]M. W. McCorquodale and R. J. Munro, "A method for reducing mean flow in oscillating-grid turbulence," Exp. Fluids **59**, 182 (2018).
[43]B. A. Toms, "Some observation on the flow of linear polymer solutions through straight tubes at large Reynolds numbers," in *Proceedings of the First International Congress on Rheology* (J. G. Oldroyd, Scheveningen, 1948), Vol. 2, pp. 135–141.
[44]E. van Doorn, C. M. White, and K. R. Sreenivasan, "The decay of grid turbulence in polymer and surfactant solutions," Phys. Fluids **11**, 2387–2393 (1999).
[45]R. H. Nadolink and W. W. Haigh, "Bibliography on skin friction reduction with polymers and other boundary-layer additives," Appl. Mech. Rev. **48**, 351–460 (1995).
[46]J. L. Lumley, "Drag reduction by additives," Annu. Rev. Fluid Mech. **1**, 367–384 (1969).
[47]K. R. Sreenivasan and C. M. White, "The onset of drag reduction by dilute polymer additives, and the maximum drag reduction asymptote," J. Fluid Mech. **409**, 149–164 (2000).
[48]P. S. Virk, "Drag reduction fundamentals," AIChE J. **21**, 625–656 (1975).
[49]P. S. Virk and D. L. Wagger, "Aspects of mechanisms in type B drag reduction," in *Structure of Turbulence and Drag Reduction*, International Union of Theoretical and Applied Mechanics, edited by A. Gyr (Springer, Berlin, Heidelberg, 1990), pp. 201–213.
[50]P. S. Virk, "Drag reduction by collapsed and extended polyelectrolytes," Nature **253**, 253109a0 (1975).
[51]M. Tabor and P. G. de Gennes, "A cascade theory of drag reduction," Europhys. Lett. **2**, 519 (1986).
[52]M. D. Warholic, H. Massah, and T. J. Hanratty, "Influence of drag-reducing polymers on turbulence: Effects of Reynolds number, concentration and mixing," Exp. Fluids **27**, 461–472 (1999).
[53]M. D. Warholic, D. K. Heist, M. Katcher, and T. J. Hanratty, "A study with particle-image velocimetry of the influence of drag-reducing polymers on the structure of turbulence," Exp. Fluids **31**, 474–483 (2001).
[54]H.-D. Xi, E. Bodenschatz, and H. Xu, "Elastic energy flux by flexible polymers in fluid turbulence," Phys. Rev. Lett. **111**, 039901 (2013).
[55]M. Q. Nguyen, A. Delache, S. Simoëns, W. J. T. Bos, and M. EL Hajem, "Small scale dynamics of isotropic viscoelastic turbulence," Phys. Rev. Fluids **1**, 083301 (2016).
[56]E. De Angelis, C. M. Casciola, R. Benzi, and R. Piva, "Homogeneous isotropic turbulence in dilute polymers," J. Fluid Mech. **531**, 1–10 (2005).
[57]G. Cocconi, E. De Angelis, B. Frohnapfel, M. Baevsky, and A. Liberzon, "Small scale dynamics of a shearless turbulent/non-turbulent interface in dilute polymer solutions," Phys. Fluids **29**, 075102 (2017).
[58]A. Liberzon, M. Guala, B. Lüthi, W. Kinzelbach, and A. Tsinober, "Turbulence in dilute polymer solutions," Phys. Fluids **17**, 031707 (2005).
[59]A. Liberzon, M. Guala, W. Kinzelbach, and A. Tsinober, "On turbulent kinetic energy production and dissipation in dilute polymer solutions," Phys. Fluids **18**, 125101 (2006).
[60]A. Liberzon, "On the effects of dilute polymers on driven cavity turbulent flows," Int. J. Heat Fluid Flow **32**, 1129–1137 (2011).
[61]A. M. Crawford, N. Mordant, H. Xu, and E. Bodenschatz, "Fluid acceleration in the bulk of turbulent dilute polymer solutions," New J. Phys. **10**, 123015 (2008).
[62]S. Rahgozar and D. E. Rival, "On turbulence decay of a shear-thinning fluid," Phys. Fluids **29**, 123101 (2017).
[63]W.-H. Cai, F.-C. Li, H.-N. Zhang, X.-B. Li, B. Yu, J.-J. Wei, Y. Kawaguchi, and K. Hishida, "Study on the characteristics of turbulent drag-reducing channel flow by particle image velocimetry combining with proper orthogonal decomposition analysis," Phys. Fluids **21**, 115103 (2009).
[64]V. K. Gupta, R. Sureshkumar, and B. Khomami, "Passive scalar transport in polymer drag-reduced turbulent channel flow," AIChE J. **51**, 1938–1950 (2005).
[65]O. Bentata, D. Anne-Archard, and P. Brancher, "Experimental study of low inertia vortex rings in shear-thinning fluids," Phys. Fluids **30**, 113103 (2018).
[66]N. Cagney and S. Balabani, "Taylor-Couette flow of shear-thinning fluids," Phys. Fluids **31**, 053102 (2019).
[67]A. G. Fabula, "An experimental study of grid turbulence in dilute high-polymer solutions," Ph.D. thesis, The Pennsylvania State University, University Park, PA, 1966.
[68]B. J. S. Barnard and R. H. J. Sellin, "Grid turbulence in dilute polymer solutions," Nature **222**, 1160–1162 (1969).
[69]C. A. Greated, "Effect of polymer additive on grid turbulence," Nature **224**, 1196–1197 (1969).
[70]C. A. Friehe and W. H. Schwarz, "Grid-generated turbulence in dilute polymer solutions," J. Fluid Mech. **44**, 173–193 (1970).
[71]W. D. McComb, J. Allan, and C. A. Greated, "Effect of polymer additives on the small-scale structure of grid-generated turbulence," Phys. Fluids **20**, 873–879 (1977).

Published under license by AIP Publishing

[72]A. B. Rodd, D. E. Dunstan, and D. V. Boger, "Characterisation of xanthan gum solutions using dynamic light scattering and rheology," Carbohydr. Polym. **42**, 159–174 (2000).
[73]F. Garcia-Ochoa, V. E. Santos, J. A. Casas, and E. Gomez, "Xanthan gum: Production, recovery, and properties," Biotechnol. Adv. **18**, 549–579 (2000).
[74]T. Lacassagne, "Oscillating grid turbulence and its influence on gas liquid mass transfer and mixing in non-Newtonian media," Ph.D. Thesis, University of Lyon, INSA, Lyon, 2018.
[75]G. Cuvelier and B. Launay, "Concentration regimes in xanthan gum solutions deduced from flow and viscoelastic properties," Carbohydr. Polym. **6**, 321–333 (1986).
[76]N. B. Wyatt and M. W. Liberatore, "Rheology and viscosity scaling of the polyelectrolyte xanthan gum," J. Appl. Polym. Sci. **114**, 4076–4084 (2009).
[77]E. A. Variano, E. Bodenschatz, and E. A. Cowen, "A random synthetic jet array driven turbulence tank," Exp. Fluids **37**, 613–615 (2004).
[78]Q. Xiao, N. Yang, J. Zhu, and L. Guo, "Modeling of cavern formation in yield stress fluids in stirred tanks," AIChE J. **60**, 3057–3070 (2014).
[79]T. Lacassagne, S. Simoens, M. EL Hajem, and J.-Y. Champagne, "Turbulence near gas-liquid interfaces in shear-thinning dilute polymer solutions" (submitted).
[80]N. T. Ouellette, H. Xu, and E. Bodenschatz, "Bulk turbulence in dilute polymer solutions," J. Fluid Mech. **629**, 375–385 (2009).
[81]N. B. Wyatt, C. M. Gunther, and M. W. Liberatore, "Drag reduction effectiveness of dilute and entangled xanthan in turbulent pipe flow," J. Non-Newtonian Fluid Mech. **166**, 25–31 (2011).
[82]J. I. Sohn, C. A. Kim, H. J. Choi, and M. S. Jhon, "Drag-reduction effectiveness of xanthan gum in a rotating disk apparatus," Carbohydr. Polym. **45**, 61–68 (2001).
[83]A. S. Pereira, R. M. Andrade, and E. J. Soares, "Drag reduction induced by flexible and rigid molecules in a turbulent flow into a rotating cylindrical double gap device: Comparison between poly (ethylene oxide), polyacrylamide, and xanthan gum," J. Non-Newtonian Fluid Mech. **202**, 72–87 (2013).
[84]H.-W. Bewersdorff and R. P. Singh, "Rheological and drag reduction characteristics of xanthan gum solutions," Rheol. Acta **27**, 617–627 (1988).
[85]M. Milas, W. F. Reed, and S. Printz, "Conformations and flexibility of native and re-natured xanthan in aqueous solutions," Int. J. Biol. Macromol. **18**, 211–221 (1996).

Published under license by AIP Publishing